

# Modelling the composition of a young star cluster ejecta

Mercedes Mollá <sup>1</sup>\* and Roberto Terlevich <sup>2,3</sup> †

<sup>1</sup> *Departamento de Investigación Básica, CIEMAT, Avda. Complutense 40. E-28040 Madrid. (Spain)*

<sup>2</sup> *INAOE, Luis Enrique Erro 1, Tonanzintla, Puebla 72840, (Mexico)*

<sup>3</sup> *Institute of Astronomy, University of Cambridge, Madingley Road, Cambridge, CB3 0HA, (UK)*

Accepted Received ; in original form

## ABSTRACT

We have computed with a fine time grid the evolution of the elemental abundances of He, C, N and O ejected by young ( $t < 20$  Myr) and massive ( $M = 10^6 M_{\odot}$ ) coeval stellar cluster with a Salpeter initial mass function (IMF) over a wide range of initial abundances. Our computations incorporate the mass loss from massive stars ( $M \geq 30 M_{\odot}$ ) during their wind phase including the Wolf-Rayet phase and the ejecta from the core collapse supernovae. We find that during the Wolf-Rayet phase ( $t < 5$  Myr) the cluster ejecta composition suddenly becomes vastly over-abundant in N for all initial abundances and in He, C, and O for initial abundances higher than 1/5th Solar. The C and O abundance in the cluster ejecta can reach over 50 times the solar value with important consequences for the chemical and hydrodynamical evolution of the surrounding ISM.

**Key words:** galaxies: abundances – stars: abundances – stars: mass-loss – stars: Wolf-Rayet –stars: supernova – galaxies: stars clusters

## 1 INTRODUCTION

Massive young stellar clusters are ideal laboratories for research into the evolution of massive stars and their interaction with their surrounding interstellar medium (ISM). These luminous and rapidly evolving massive stars supply most of the young cluster UV radiation that creates the encompassing HII region and a large amount of mass and mechanical energy in the forms of supernova ejecta and stellar winds particularly during the WR phase. These massive starforming regions can eject during their first 10 Myr of evolution about 20% of their initial mass (Leitherer et al., 1999) (hereinafter STB99) mostly in the form of newly synthesized C, N and O that by mass represent most of the heavy elements.

Massive young stellar clusters are ubiquitous particularly among late type galaxies. Their stellar wind phase can result in a supergalactic wind affecting the nearby intergalactic medium (IGM). It is open to question how the ejected freshly synthesized heavy elements cools and mix with the ISM, and how long this process governed by the cooling time scale, may last. The time scale for cooling is strongly dependent on the gas cooling rate that in turn is dependent on the gas chemical composition and density (e.g. Tenorio-Tagle, 1996; Kobulnicky et al., 1997; Kobulnicky & Skillman, 1998; van Zee & Haynes, 2006; López-Sánchez & Esteban, 2010). Thus evaluating the composition of the cluster ejecta and its time evolution is a necessary prior step for estimates of the evolution of the cooling function and

the computation of cooling and feedback time scales. Although work like that of Silich et al. (2001) underlined the large influence that the enrichment of the stellar ejecta can have on the radiative cooling of starburst superbubbles, many researchers are still using Raymond et al. (1976) radiative cooling coefficient calculation for Solar abundances when modelling the interaction between the stellar ejecta and their surrounding medium.

In this paper we present a set of models designed to calculate in detail the first 20 Myr of the evolution and chemical composition of a star cluster ejecta on very short time scales, i.e. much shorter than the HII region lifetime and in particular to resolve the WR wind phase

Galactic chemical evolution models traditionally assume that the elements ejected by the stellar cluster are incorporated to the ISM when the corresponding stars die, i.e. at a time equal to their lifetimes (Portinari, Chiosi, & Bressan, 1998; Dray & Tout, 2003; Dray et al., 2003). The shortest time step is usually defined by the mean-lifetime of the most massive star. Since this is typically around 100–120 Myr, chemical evolution calculations begin normally at around 3–5 Myr with comparable time-steps. This way important phases of the wind evolution, occurring before 3 Myr or short lived like the WR phase are lost or diluted.

To compute the composition of the ejecta, most chemical evolution models use the total yields of elements due to supernova explosions, such as those given by Woosley & Weaver (1995, WW95) or other more recent works (Umeda & Nomoto, 2002; Rauscher et al., 2002; Limongi & Chieffi, 2003; Chieffi & Limongi, 2004; Fröhlich et al., 2006; Heger & Woosley, 2010) to calculate the total change of the elemental abun-

\* E-mail: mercedes.molla@ciemat.es

† Visiting Professor UAM, Madrid

dances. Other computations include the elements ejected during the wind phase of massive stars (Maeder, 1992; Meynet & Maeder, 2002; Hirschi, Meynet, & Maeder, 2005; Hirschi, 2007; Kobayashi et al., 2006), only the models of Portinari, Chiosi, & Bressan (1998, hereinafter PCB98) include the evolution of both phases, i.e. the yields of core collapse supernova explosions from Woosley & Weaver (1995) and the stellar wind yields produced during the evolution of each star. However, PCB98 computations, as most chemical evolution models, were performed with time steps much longer than the lifetime of an HII region therefore missing short lived stages like the WR phase. Moreover, the evolution of a supernova progenitor that loses part or most of its mass is not the same as a normal main sequence massive star. Since mass and structure are substantially different in the time of the supernova explosion, the associated yields will also differ, such as it is explained in Woosley et al (1993); Woosley, Langer & Weaver (1995, hereinafter WLW93 and WLW95, respectively). To take this into account, PCB98 linked the final stage of the star after lost mass with the supernova yields though the CO core mass. However, they use the WW95 yields instead WLW93/WLW95 yields.

The organization of this paper is as follows: In Section 2 we use O and WR winds computations to estimate the evolution of the ejecta of a young massive stellar cluster. In section 3 we compute the contribution of the explosive nucleosynthesis. Section 4 gives the complete evolution of elemental abundances within the cluster and discusses the impact of each contribution phase over the final ejecta. Our conclusions are given in Section 5.

## 2 STELLAR WIND COMPOSITION

To compute the evolution of the rate of ejection of elements due to stellar winds of a Single Stellar Population (SSP) of a given initial metallicity and initial mass function (IMF), we have used the tables resulting from the isochrones calculation by Bressan, Bertelli & Chiosi (1993); Fagotto et al. (1994a,b). These authors give the amount of mass lost by massive stars during their evolution for 7 initial stellar masses: 12, 15, 20, 30, 40, 60 and 100  $M_{\odot}$ . For each initial mass and time step, the tables provide the present mass (in solar mass units), the rate of mass loss in  $M_{\odot} \text{ yr}^{-1}$  (logarithmic scale) and the abundances of the stellar surface for H,  $^4\text{He}$ ,  $^{12}\text{C}$ ,  $^{14}\text{N}$ , and  $^{16}\text{O}$ . These tables are provided for 6 initial metallicities:  $Z=0.0001, 0.0004, 0.004, 0.008, 0.02$  and  $0.05$ .

In Fig. 1 we plot the evolution of the mass loss rate for all stellar masses. The mass loss rate depends strongly on the initial stellar mass and composition. It is clear from the figure that the lowest mass stars maintain for a long time a low mass loss rate while the most massive ones evolve rapidly ejecting a large part of their mass in discrete events. An important consequence is that a star of solar metallicity with an initial mass of 100  $M_{\odot}$  ends its life with around 7  $M_{\odot}$ , while the evolution of star of 12  $M_{\odot}$  may be followed for almost 20 Myr at a very low mass loss rate that implies that its total mass remains roughly constant.

The mass loss rate is also dependent on the metallicity through the semi-empirical relation included in the stellar models (see Bressan, Bertelli & Chiosi, 1993, for details). We see these differences in Fig. 1 where the evolution for the 6 given metallicities stars are shown. The lower the metallicity, the smaller the mass loss rate and smoother the behavior shown on the mass loss rate evolution.

In Table 1 we summarize some characteristics of the stellar input models: For each metallicity  $Z$ , column 1, and initial stellar

**Table 1.** Characteristics of the stellar models

$Z$	$m_*$ ( $M_{\odot}$ )	$m_{end}$ ( $M_{\odot}$ )	$t_{end}$ (Myr)	$X_{f,H}$
0.0001	12	11.99	21.17	0.748
0.0001	15	14.98	15.28	0.731
0.0001	20	19.93	10.65	0.701
0.0001	30	29.69	7.00	0.770
0.0001	40	38.93	5.52	0.770
0.0001	60	37.31	4.19	0.681
0.0001	100	67.39	3.18	0.649
0.0004	12	11.97	21.39	0.741
0.0004	15	14.94	15.39	0.727
0.0004	20	19.83	10.64	0.699
0.0004	30	29.35	6.91	0.673
0.0004	40	35.66	5.46	0.693
0.0004	60	31.89	4.20	0.486
0.0004	100	55.45	3.32	0.142
0.004	12	11.84	21.47	0.716
0.004	15	14.76	15.26	0.705
0.004	20	19.30	10.48	0.686
0.004	30	19.05	6.86	0.544
0.004	40	16.86	5.44	0.241
0.004	60	17.55	4.20	0.000
0.004	100	46.93	3.38	0.080
0.008	12	11.77	21.07	0.708
0.008	15	14.62	14.92	0.693
0.008	20	19.03	10.10	0.671
0.008	30	13.05	6.66	0.516
0.008	40	16.44	5.31	0.000
0.008	60	10.87	4.22	0.000
0.008	100	14.23	3.44	0.000
0.02	12	11.50	18.93	0.667
0.02	15	14.21	13.34	0.655
0.02	20	18.06	9.17	0.630
0.02	30	12.63	6.15	0.000
0.02	40	5.35	5.14	0.000
0.02	60	6.01	4.13	0.000
0.02	100	7.16	3.40	0.000
0.05	12	10.85	13.95	0.577
0.05	15	13.12	9.97	0.565
0.05	20	16.05	6.99	0.539
0.05	30	9.84	5.15	0.000
0.05	40	3.63	4.36	0.000
0.05	60	4.11	3.63	0.000
0.05	100	4.22	3.11	0.000

mass  $m_*$ , column 2, the final mass  $m_{end}$  is listed in column 3, and the final evolutionary time  $t_{end}$  in Myr is in column 4. Column 5 shows the final surface abundance (in mass fraction) of H,  $X_{f,H}$  (which we will use to determine the mass of the Helium core in section 3).

Since each stellar mass table has a different time range and step, we have performed a linear interpolation to obtain values at the same times for all masses. The normalized table is provided in electronic format for all calculated metallicities and masses. Table 2 shows as an example, a few time steps of the most massive star of  $Z=0.02$ . It gives for the metallicity of column 1, and for the seven stellar masses, defined by column 2, the initial mass  $m_*$  in solar mass units in column 3, the time in Myr units in column 4, the mass loss rate,  $\dot{m}$ , in units of solar mass per year, in column 5, the elemental abundances of H,  $^4\text{He}$ ,  $^{12}\text{C}$ ,  $^{14}\text{N}$ , and  $^{16}\text{O}$ <sup>1</sup> as fractions in

<sup>1</sup> For the sake of simplicity we write He, C, N and O for  $^4\text{He}$ ,  $^{12}\text{C}$ ,  $^{14}\text{N}$ , and  $^{16}\text{O}$  along the text.

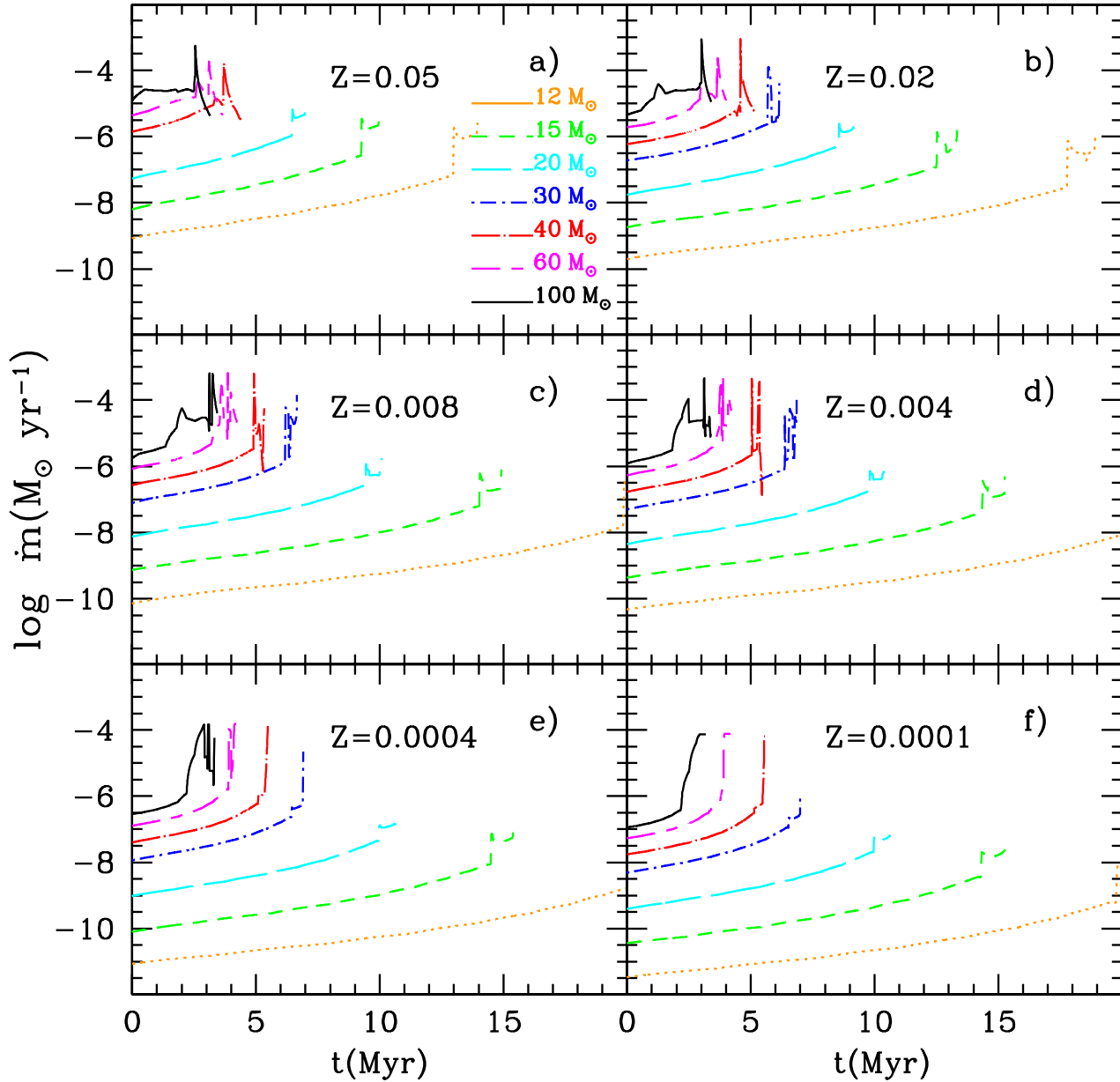


**Figure 1.** Evolution of the mass loss rate for the stars given by the Padova group for different metallicities  $Z$  as labelled. Color and type of lines mean a different value of stellar mass as labelled.

**Table 2.** Surface abundances of the stellar models for each mass for  $Z=0.02$ . Similar complete tables for the six metallicities and seven stellar masses will be provided in electronic format

$Z$	$N$	$m_*$ ( $M_\odot$ )	$t$ (Myr)	$\dot{m}$ $M_\odot \cdot \text{yr}^{-1}$	XH	XHe	XC	XN	XO	$m(t)$ ( $M_\odot$ )
0.02	7	100.	1.300	0.364E-04	0.687E+00	0.293E+00	0.434E-02	0.271E-02	0.963E-02	87.49
0.02	7	100.	1.310	0.358E-04	0.684E+00	0.296E+00	0.418E-02	0.312E-02	0.937E-02	87.25
0.02	7	100.	1.320	0.351E-04	0.680E+00	0.300E+00	0.402E-02	0.353E-02	0.911E-02	87.00
0.02	7	100.	1.330	0.345E-04	0.676E+00	0.304E+00	0.386E-02	0.394E-02	0.885E-02	86.76
0.02	7	100.	1.340	0.338E-04	0.672E+00	0.308E+00	0.370E-02	0.435E-02	0.859E-02	86.51
0.02	7	100.	1.350	0.332E-04	0.668E+00	0.312E+00	0.354E-02	0.476E-02	0.832E-02	86.27
0.02	7	100.	1.360	0.325E-04	0.664E+00	0.316E+00	0.338E-02	0.518E-02	0.806E-02	86.02

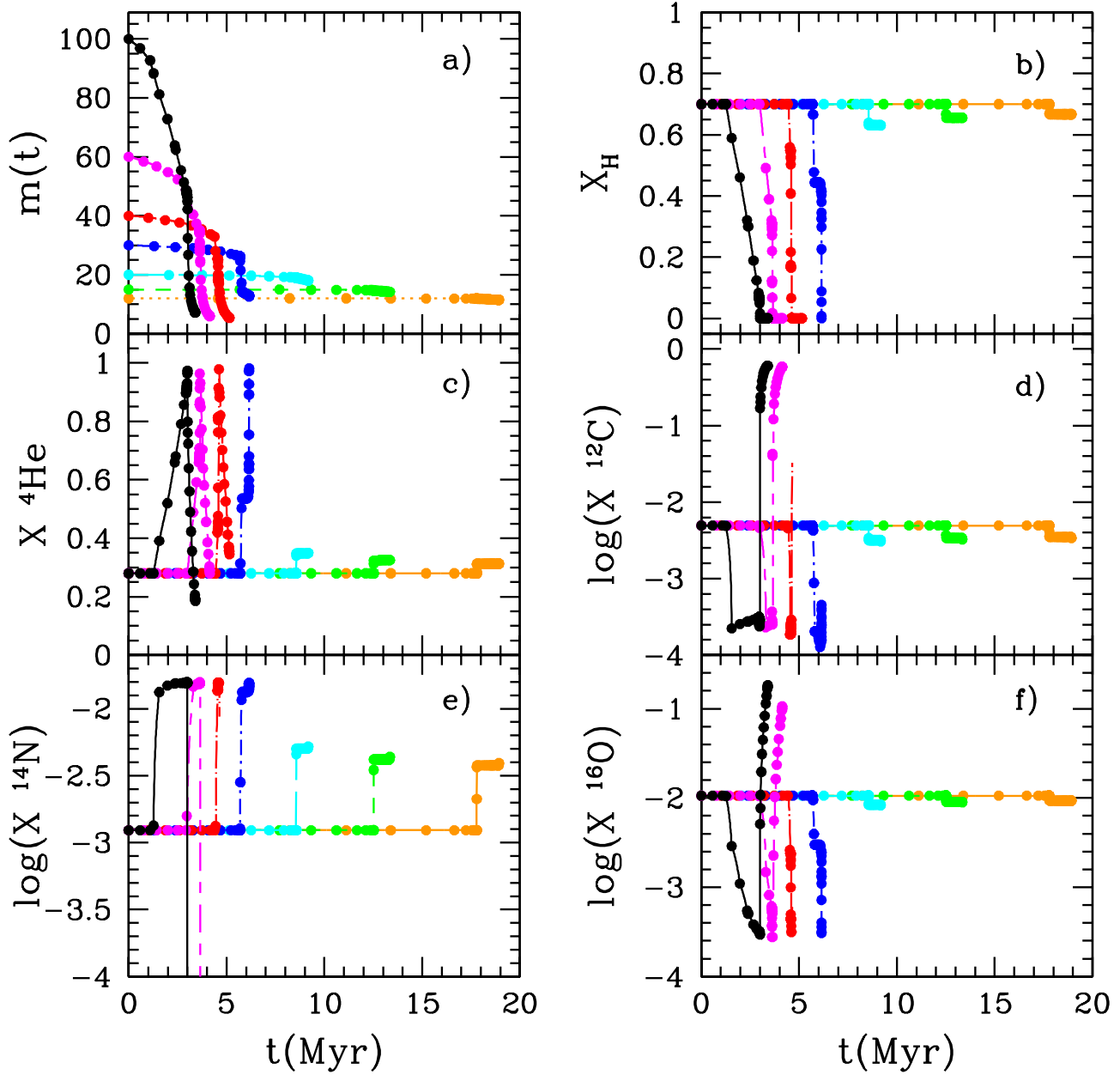


**Figure 2.** Input stellar parameters for  $Z=0.02$ . The evolution of the stellar mass is shown in panel (a) and the evolution of the surface abundances is shown in panels (b) to (f) for the same initial stellar masses as labelled in Fig. 1. The dots represent the actual results from the stellar evolutionary models while the lines are the interpolation in time used in this work.

mass, in columns 6 to 10, and the stellar mass  $m(t)$  at a given time  $t$ , in column 11.

The evolution of the stellar masses and surface abundances is shown with dots in Fig. 2. Each type and color of line indicate a stellar mass as labelled. The lines shows the results of the numerical interpolation used in the following sections. In panel a) we see how drastically the stellar mass decreases when  $m > 30M_{\odot}$  in times as short as 5 Myr. The evolution of the stellar surface abundances for H, He in total mass fraction and C, N, and O, as abundances in mass,  $X$ , is shown in panels b) to f) of the same Fig. 2. The surface abundances of C, N and O show a large increase following the

start of the stellar winds revealing the the product of first hydrogen and then helium burning. This fact combined with a depletion of H in the ejecta means that, if these abundances were represented as abundances in number,  $12 + \log(X/H)$ , they would be very high.

To compute the evolution of a stellar cluster ejecta we have assumed that the cluster stellar mix consists of a coeval population or single stellar population (SSP) where all stars were created simultaneously and with the same metallicity. By using the normalized tables of the previous paragraph, it is easy to calculate in each time step the contribution of each star,  $m$ , weighted by the number

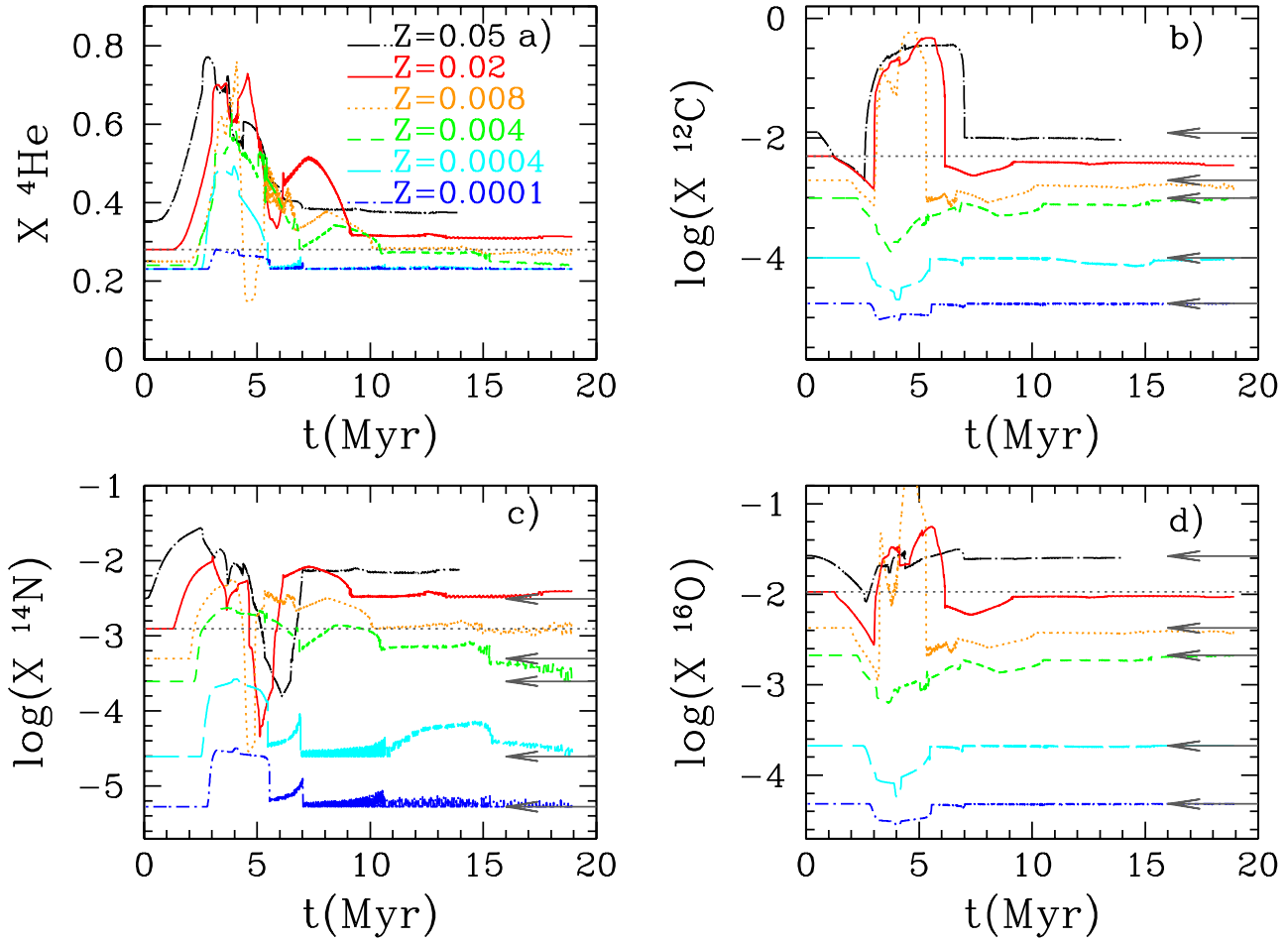


**Figure 3.** Evolution of the instantaneous abundances in mass for a stellar cluster due to stellar wind integrated for a Salpeter IMF: a) He, b) C, c) N and d) O for  $Z=0.05, 0.02, 0.008, 0.004, 0.0004$  and  $0.0001$  with different coded lines as labelled in panel a. In each panel the dotted grey line marks the initial abundance for  $Z=0.02$  and the arrows the initial values for the other metallicities

of stars in its mass range, given by the initial mass function  $\Phi(m)$ . Thus, for each element  $i$  and each time  $t$ :

$$m_{e,ji}(t) = \int_{m_{low}}^{m_{up}} \int_{\Delta t} e_{z,i}(m, t') \phi(m) dm dt' \quad (1)$$

where

$$e_{z,i}(m, t') = XS_i(m, t') \dot{m}(t') \quad (2)$$

$XS_i(m, t)$  is the surface abundance of each element  $i$  and  $\dot{m}(t)$  is the mass loss rate for each stellar mass  $m$  in every time  $t$ .

We have performed the calculations for 6 different initial mass functions: 1) A Salpeter (1955) law,  $\Phi(m) \propto m^{-x}$ , with an exponent  $x = -2.35$  (hereinafter SAL), and 5 others from: 2) Miller & Scalo (hereinafter MIL 1979), 3) Ferrini, Penco, & Palla (1990, hereinafter FER), 4) Kroupa (hereinafter KRO 2001), and 5) Chabrier (hereinafter CHA 2003); all of them with limits  $m_{low} = 0.15$  and  $m_{max} = 100 M_{\odot}$  and 6) a Salpeter law with limits  $m_{low} = 1.00$  and  $m_{max} = 100 M_{\odot}$  as the one used in STB99. Our tables are therefore calculated for all these IMFs, but in the next figures only Salpeter results are shown since it is a widely used IMF.

The integration is done for the whole mass range of the IMF in each time step. To integrate in time we have chosen a time step  $\delta t = 0.01$  Myr (small enough to follow the rapid evolution of the

mass loss process without losing any phase). To integrate in mass it is necessary to be available a grid with a wide range of masses. So, we have performed a careful interpolation in mass using the 7 existing tables. The method to obtain the mass loss rate for any mass value it is not straightforward, since it shows abrupt changes in small time scales. So we have used the tables of the mass loss rate to calculate the actual mass  $m(t)$  in any time with high accuracy. Then we have interpolated between these values for obtaining a new curve for each mass  $m$ , and finally we compute the mass loss rate from this  $m(t)$ . To calculate the elemental abundances, we have taken into account the different phases of each element abundance, interpolating between two known masses to obtain the points limiting these phases for each mass  $m$ . All computations were done for a SSP cluster with a total mass in stars of  $10^6 M_{\odot}$ .

In Fig. 3 we show the resulting evolution of the instantaneous ejecta abundances  $X$  for He, C, N and O in mass as before. Initial

<sup>2</sup> It is necessary to take into account that we will give averaged values for this stellar cluster mass. For stellar clusters less massive than  $10^4 M_{\odot}$ , the stochastic effects over the initial mass function are important (Cerviño & Luridiana, 2004, 2006) and they may change the stellar mass distribution and the corresponding results compared with those we obtain.

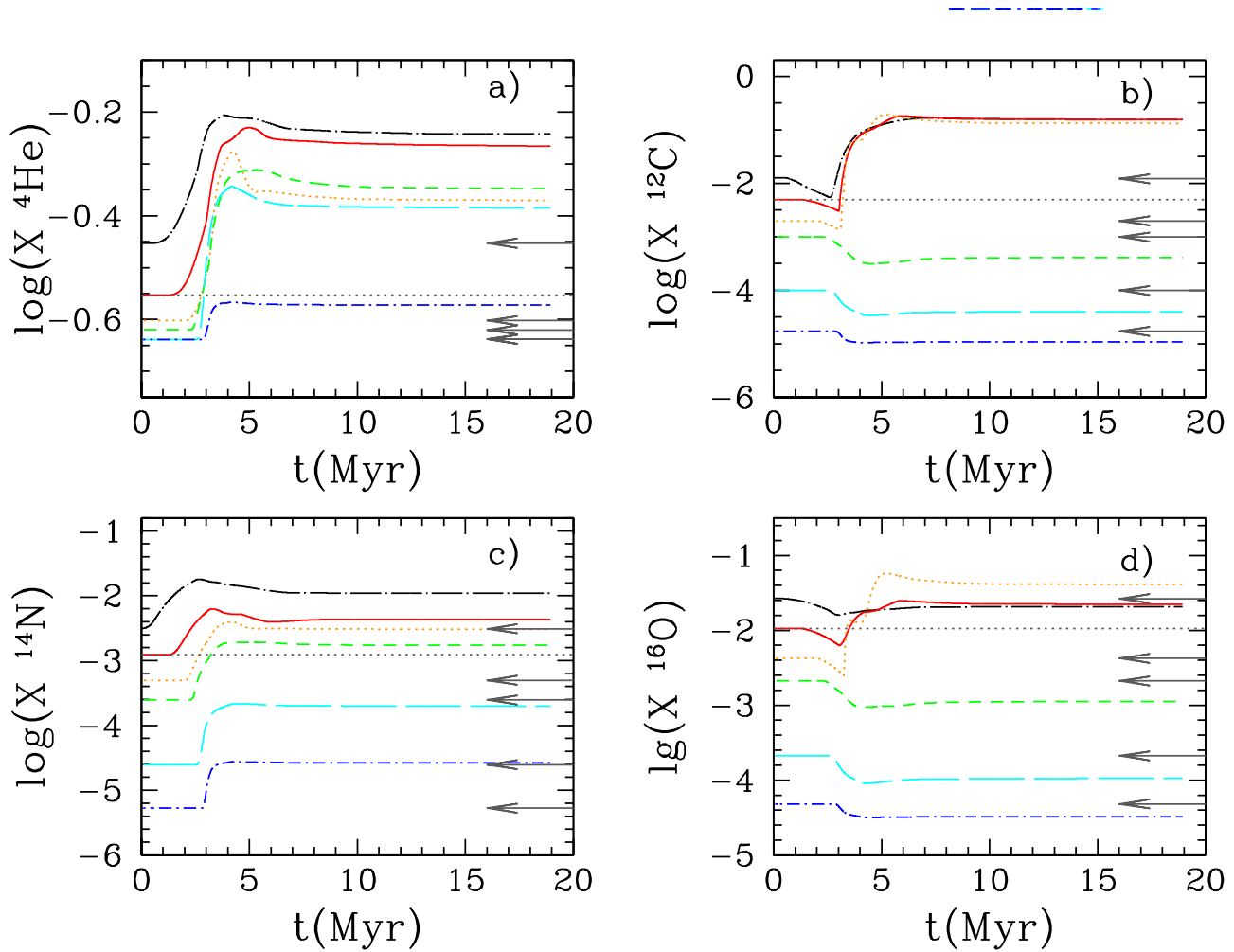


**Figure 4.** Evolution of abundances in mass of the accumulated masses ejected by a stellar cluster for a) He, b) C, c) N and d) O. The metallicities are shown with the same color codes as in the previous figure. The dotted line and the arrows have the same meaning than in Fig. 3

**Table 3.** Accumulated Masses ejected by a stellar cluster of  $10^6 M_{\odot}$  during its wind phase for 20 Myr for  $Z=0.02$  and a Salpeter IMF. The complete tables for all times, metallicities and IMFs will be provided in electronic format

IMF	Z	time (Myr)	$m_{ej}$ ( $M_{\odot}$ )	H ( $M_{\odot}$ )	He ( $M_{\odot}$ )	C ( $M_{\odot}$ )	N ( $M_{\odot}$ )	O ( $M_{\odot}$ )
SAL	0.0200	0.50	0.753E+03	0.527E+03	0.210E+03	0.372E+01	0.934E+00	0.798E+01
SAL	0.0200	0.51	0.770E+03	0.539E+03	0.215E+03	0.380E+01	0.954E+00	0.816E+01
SAL	0.0200	0.52	0.787E+03	0.550E+03	0.220E+03	0.388E+01	0.975E+00	0.834E+01
SAL	0.0200	0.53	0.804E+03	0.562E+03	0.225E+03	0.397E+01	0.996E+00	0.852E+01
SAL	0.0200	0.54	0.821E+03	0.574E+03	0.229E+03	0.405E+01	0.101E+01	0.870E+01
SAL	0.0200	0.55	0.838E+03	0.586E+03	0.234E+03	0.414E+01	0.103E+01	0.888E+01
SAL	0.0200	0.56	0.855E+03	0.598E+03	0.239E+03	0.422E+01	0.106E+01	0.906E+01
SAL	0.0200	0.57	0.872E+03	0.610E+03	0.244E+03	0.430E+01	0.108E+01	0.924E+01

abundances are the ones included in the original files for  $Z=0.0001$ , 0.0004, 0.004, 0.008, 0.02 and 0.05. If we take the solar abundances from Asplund et al. (2009) as reference, which implies a total  $Z_{\odot} = 0.0142$ , the  $Z=0.02$  abundances, indicated in the figure as dotted grey lines, are in fact  $\sim 0.15$  dex higher than the adopted Solar values. If we analyze the results for  $Z=0.02$  (red lines) we see that cluster ejecta abundances are not always equal to the initial value. It is evident that ejecta abundances show strong variations in

the WR stars phase, that may reach up to two orders of magnitude over the initial value for each metallicity. Thus, He and N increase in a first phase, when C and O decrease. Then N and He decrease again just when C and O increase.

This effect is strongly dependent on the original metallicity of the stellar cluster as we may see by comparing with the other metallicity lines. The initial values for the non-solar cases are indicated with arrows around the values, +0.3, -0.4, -0.7, -1.7 and -2.3 dex.

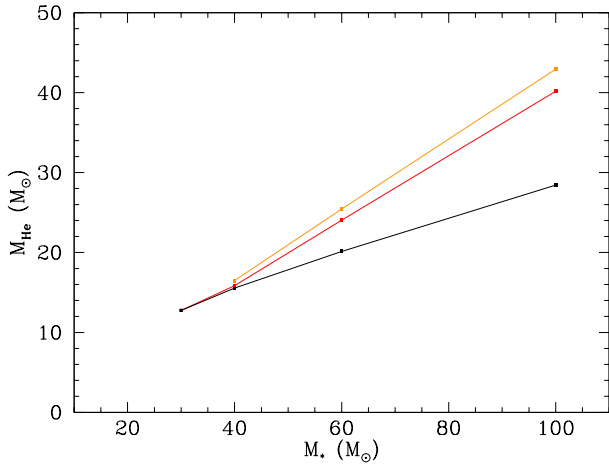


**Figure 5.** The relation between the He core mass  $m_{He}$ , defined as the stellar mass when the H abundance is zero, and the initial stellar mass at the main sequence  $m_*$  for models with  $m \geq 30 M_\odot$ . Each line corresponds to a metallicity as labelled.

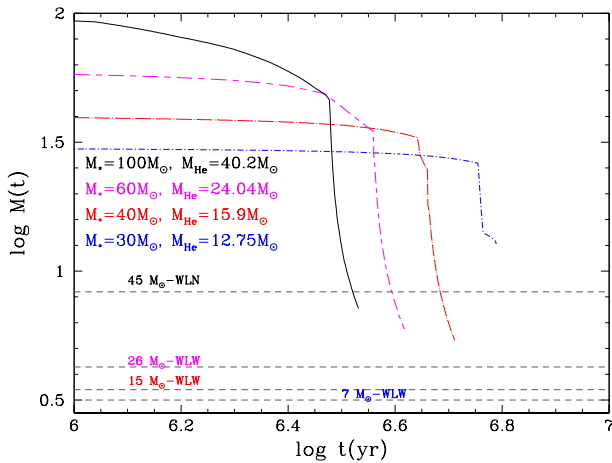


**Figure 6.** Evolution of the instantaneous mass in the higher mass stellar models. The horizontal lines give the WLV93/WLV95 final masses.

For the two models with the lowest metallicity, the ejecta abundances, in particular C and O, do not differ very much from the initial values except for the decrease around 4-5 Myr. However, for higher initial metallicities, all lines show a strong sudden increase at around 4.5-5 Myr reaching values 1 or 2 orders of magnitude larger than the initial value and lasting few million years.

For N the behavior is however different. For all models the N abundance in the ejecta increases at 3 Myr, even at the lowest metallicities. After about 5 to 8 Myr of evolution, when the cluster turnoff mass is below  $25 M_\odot$  the ejecta metallicity asymptotically approaches the initial value for all initial compositions, except again for N which maintains a higher value than the initial one. Probably this may be explained by the fact that the convective envelope dredges up the modified composition of CNO from the inner parts of the star up to the surface during the Red Supergiant (RSG) RSG phase, which enhances the N mass fraction, slightly reducing C and O abundances.

The resulting accumulated ejected masses for the cluster in every time step are given in Table 3. For each IMF, column 1, and metallicity, given in column 2, we give the time step in Myr in

**Table 4.** Relation stellar mass-He core mass for Padova stellar tracks

$m_*$	Z		
	0.008	0.02	0.05
30	...	12.05	9.84
40	17.04	14.50	15.56
60	25.44	27.80	20.13
100	45.14	42.20	28.44

column 3, the total ejected mass in column 4, and the accumulated ejected mass of the different elements in columns 5 to 9 for H, He, C, N, and O. We show an example here for solar metallicity and a Salpeter IMF, the complete tables for all times, metallicities and IMFs will be provided in electronic format.

The evolution of the accumulated ejecta abundances shows in Fig. 4 a sharp increase for  $Z \geq 0.008$  due to the mass loss of massive stars followed by a plateau after the peak of mass loss associated with the WR stars decline. For the models with the lowest metallicities, C and O abundances do not change much in relation with the initial values, as explained before, decreasing slightly, simultaneously to the increase of N. However, for the other metallicities the increase in C and O abundances is quite large. On the other hand, He and N abundances, even at the lowest metallicity cases, show the sharp increase at 3 Myr followed by a plateau that shows an enrichment with respect to the initial value larger than 0.5 dex in most cases. This increase in the He and N abundance may have important consequences for measurements of the chemical composition of galaxies based on abundances estimated using emission lines from HII regions particularly for the lowest metallicity regions i.e. those with  $12 + \log(O/H) \leq 7.3$ .

These huge variations in the abundances of the ejecta of a stellar cluster may also be important for the hydrodynamical evolution of the ISM. The high metallicity might lead to extremely short cooling times in the ejecta with important consequences for the subsequent feedback.

### 3 ADDING THE SUPERNOVA EJECTA TO THE STELLAR WINDS

In this section we include the elements produced by supernova in our calculations. Stars more massive than  $m \geq 12 M_\odot$  end their evolution as core collapse supernovae. New elements are created and ejected in these events. Since we assume an IMF where the most massive star  $m_{max} = 100 M_\odot$  has a mean lifetime of  $\tau = 3.7$  Myr, the ejections are zero before this time. Only after 3.7 Myr supernovae begin to contribute to the cluster ejected mass.

In computing the total ejected mass and its composition, an important effect to take into account is that due to the stellar wind the mass of a star at the pre-supernova stage is smaller than its main sequence mass. Thus, the supernova yields for a given star are not those corresponding its main sequence mass since the star which explodes is less massive. To estimate the supernova yields we took as the supernova progenitor mass, the mass of each star at the end of its wind phase. In practice the models behave in two different ways depending on the wind mass loss rate:

(i) *Small mass loss rate.* Stars with initial masses around  $15 M_\odot$  lose only part of their H, therefore  $X_H > 0$  at all times. For example stars with  $Z = 0.02$  and initial masses 12, 15 and  $20 M_\odot$  end the winds phase with 11.46, 14.21 and  $18.06 M_\odot$ , respectively. In this case, and even more so for smaller abundances, it is reasonable to

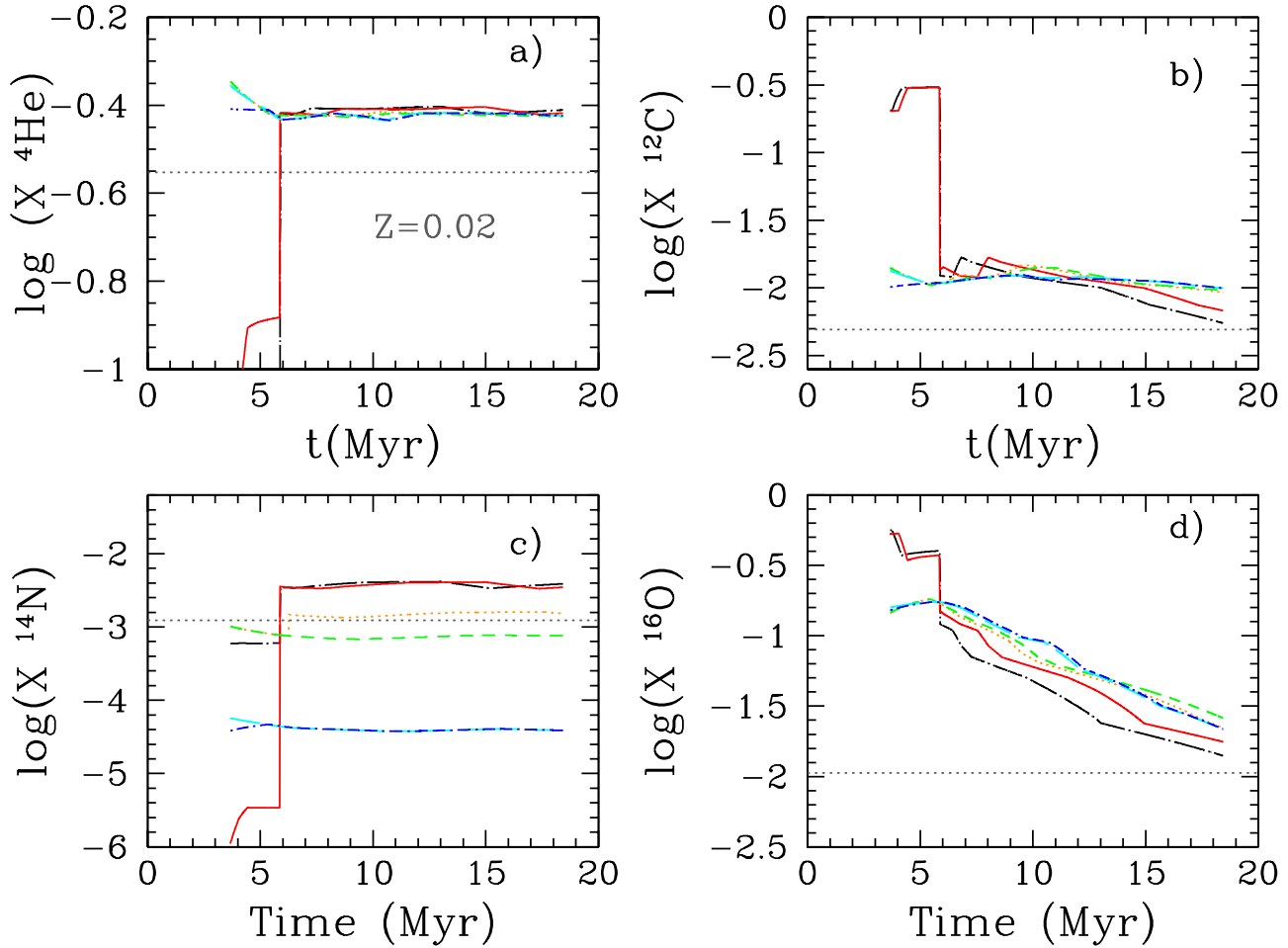


**Figure 7.** Evolution of the instantaneous values of He, C, N, and O abundances in mass in the ejecta of a stellar cluster during the supernova phase. The line codification is as in figure 4. The dotted grey line marks the abundance  $Z=0.02$  in each panel.

assign them the WW95 models in the same way as PCB98 did. In those cases we simply use the final mass of each star to select the most appropriate model among the models given by WW95.

(ii) *High mass loss rate.* Stars with  $Z \geq 0.008$  and  $M \geq 30 M_{\odot}$  have high mass loss rates and arrive to the end of the wind phase without H envelope inducing important changes to the supernova explosion mechanism and ejecta. For this case we adopted the models by Woosley et al (1993); Woosley, Langer & Weaver (1995, hereinafter WLW93 and WLW95, respectively). WLW95 calculated the evolution of stars between 4 and  $20 M_{\odot}$  without H envelope. Their results are given for a range of masses of Helium core  $m_{\text{He}}$ , defined as the mass at which the abundance of H falls to zero. After H exhaustion, these stars continue losing mass. A star of  $m_{\text{He}} = 20 M_{\odot}$  loses  $16.44 M_{\odot}$ , ending with a mass of  $3.55 M_{\odot}$ . Then, it explodes ejecting other  $2.00 M_{\odot}$  and keeping  $1.55 M_{\odot}$  in the remnant. In similar way a star of  $m_{\text{He}} = 7.00 M_{\odot}$  loses  $3.80 M_{\odot}$  ending with  $3.20 M_{\odot}$  before exploding, ejecting  $1.70 M_{\odot}$  and producing a remnant of  $1.50 M_{\odot}$ .

Using the Padova tracks we obtain for the seven original values of stellar masses, the mass of each star when H is depleted from the envelope. These values are shown in Table 4 for  $Z \geq 0.008$  given that for metallicities lower than this the condition  $X_{\text{H}} = 0$  is never reached. The relation between the initial mass in the main sequence

$m_*$  and the mass of the He core  $m_{\text{He}}$  is shown in Fig. 5 where we see that the behaviour is quite smooth with the resulting  $m_{\text{He}}$  ranging from 10 to  $45 M_{\odot}$ . The explosive yields for masses  $m_{\text{He}}$  between 4 and  $20 M_{\odot}$  are taken from WLW95. For masses higher than  $20 M_{\odot}$ , we take the results from WLW93 where the evolution of WR stars is computed starting at  $X_{\text{H}}=0.50$ . For models with initial mass of 60 and  $85 M_{\odot}$ , (which begin the RSG or Luminous Blue Variable (LBV) phase with  $55.5$  and  $76.9 M_{\odot}$ , respectively), the resulting He core masses are  $m_{\text{He}} = 26.3 M_{\odot}$  and  $45.3 M_{\odot}$ , respectively, their masses at the end of the wind phase being only  $4.25$  and  $8.30 M_{\odot}$ . These models are very similar to our most massive stars of 60 and  $100 M_{\odot}$ , for which  $m(X_{\text{H}}=0.50)$  are  $44.4$  and  $80 M_{\odot}$ , with  $m_{\text{He}} = 27.8$  and  $44.9 M_{\odot}$  and with final masses of  $5.93$  and  $7.16 M_{\odot}$ .

In Fig. 6 we show the comparison between the evolution of the most massive stars used here with the final results of WLW93/WLW95. Note that the final masses in the Padova models for  $Z=0.02$  are slightly larger than the ones from WLW95/WNL93 with the exception of the most massive model. For this case the Padova model reaches  $7.17 M_{\odot}$  at the end of the evolution while the corresponding model from WLW93 has a slightly higher value ( $8.30 M_{\odot}$ ).

Thus, to compute the explosive yields for massive stars with high mass loss rate, we proceeded as follows: for each time step of our



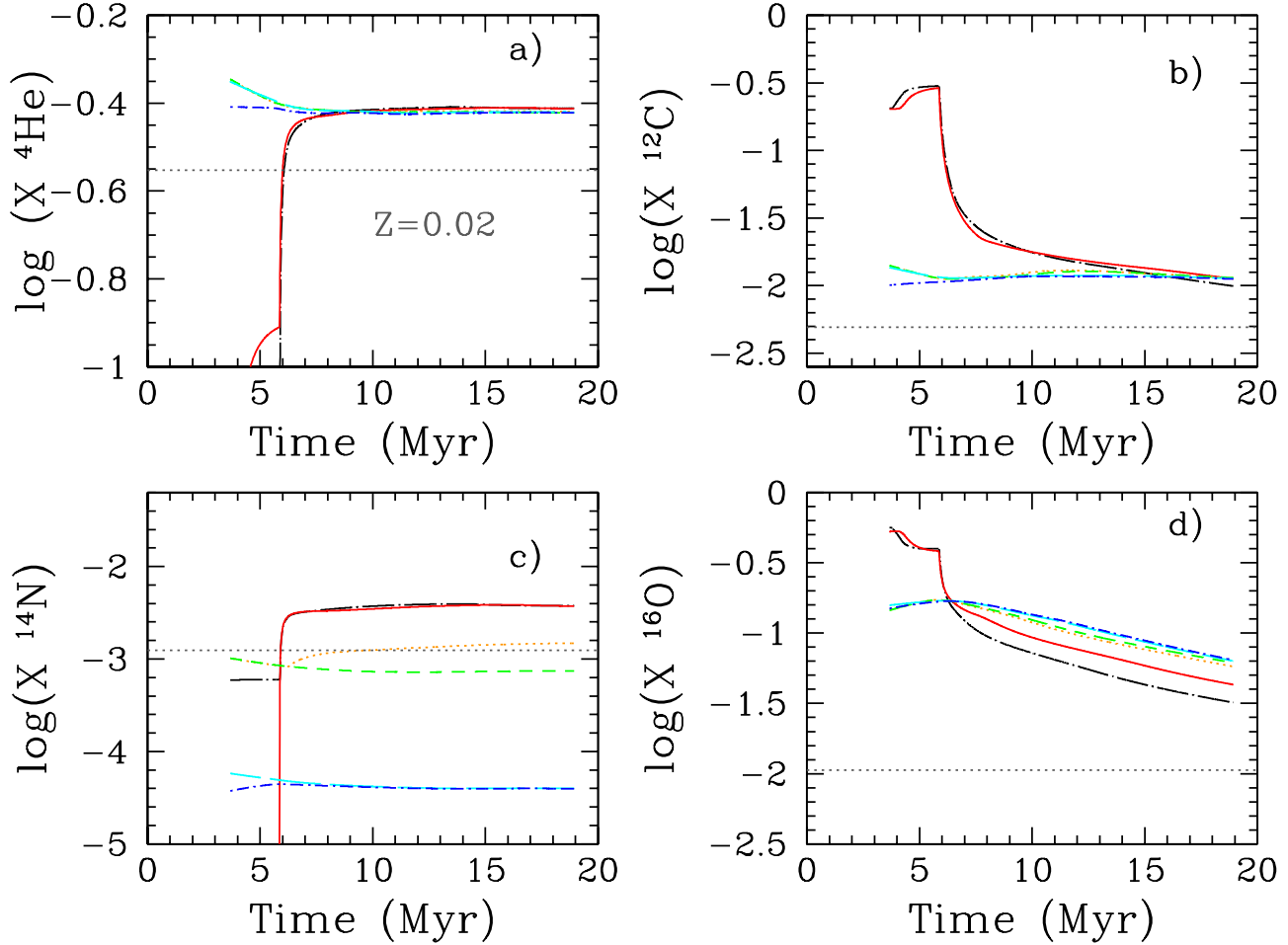


**Figure 8.** The evolution of the abundances in mass as  $\log X$  of the accumulated ejected mass by a stellar cluster during the supernova phase for a) He, b) C, c) N and d) O for  $Z=0.02$  and a Salpeter IMF. The dotted grey line marks the reference abundance in each panel.

**Table 5.** Accumulated masses ejected by stars dying as supernova explosions for a stellar cluster of  $10^6 M_{\odot}$  during the first 20 Myr for  $Z=0.02$  and a Salpeter IMF. The complete table with all times, metallicities and IMFs will be provide in electronic format.

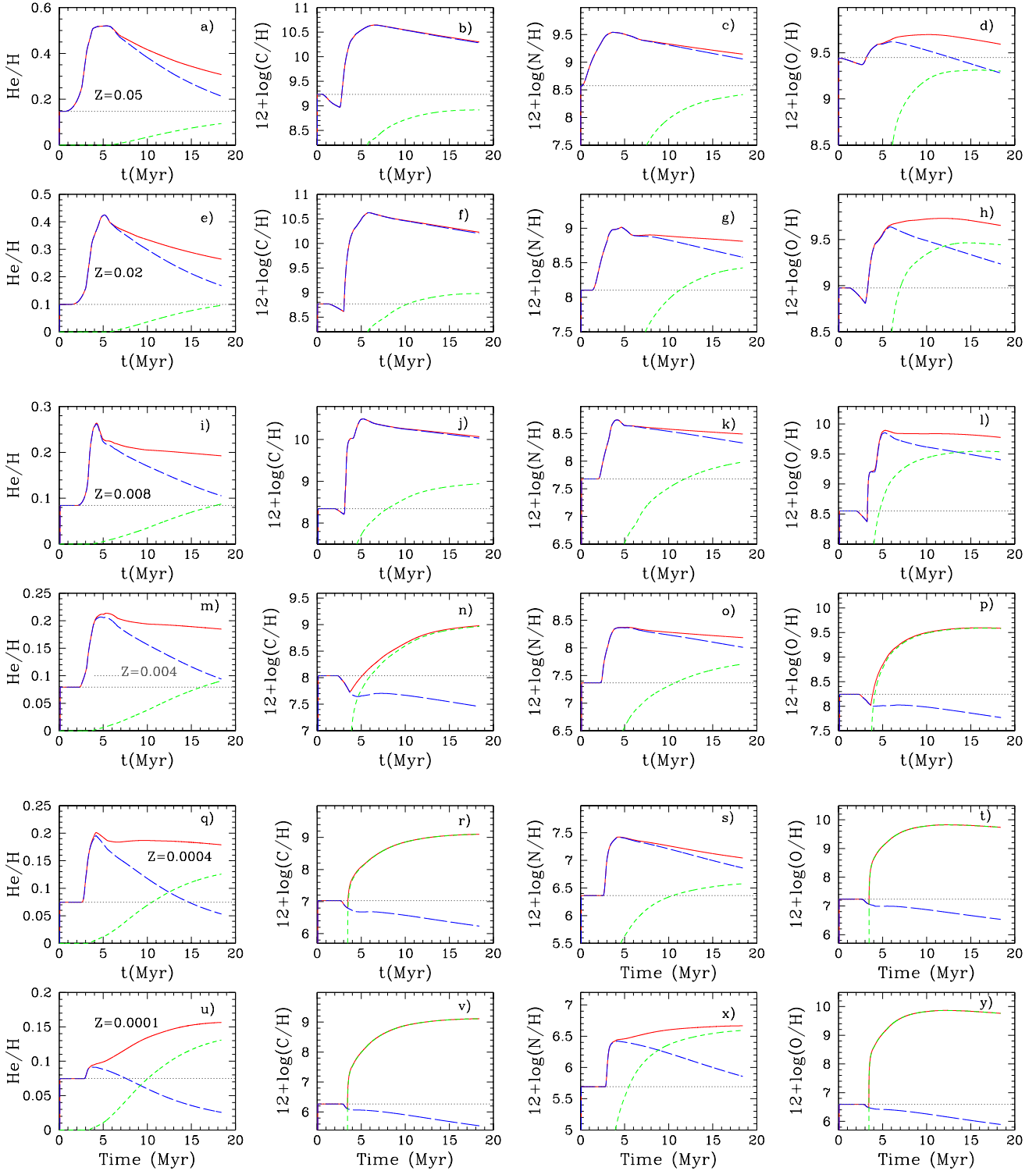
IMF	Z	time (Myr)	$m_*$ ( $M_{\odot}$ )	$m_{\text{He}}$ ( $M_{\odot}$ )	$m_{\text{rem}}$ ( $M_{\odot}$ )	$m_{\text{ej}}$ ( $M_{\odot}$ )	H ( $M_{\odot}$ )	He ( $M_{\odot}$ )	C ( $M_{\odot}$ )	N ( $M_{\odot}$ )	O ( $M_{\odot}$ )
IMF	0.02	0.37700E+01	86.5627	34.7581	1.5500	0.2452E+01	0.0000E+00	0.1971E+00	0.4966E+00	0.3056E-05	0.1295E+01
IMF	0.02	0.37800E+01	85.5161	34.3357	1.5500	0.2698E+01	0.0000E+00	0.2169E+00	0.5465E+00	0.3403E-05	0.1425E+01
IMF	0.02	0.37900E+01	84.4982	33.9250	1.5500	0.2946E+01	0.0000E+00	0.2368E+00	0.5969E+00	0.3762E-05	0.1556E+01
IMF	0.02	0.38000E+01	83.5080	33.5255	1.5500	0.3196E+01	0.0000E+00	0.2570E+00	0.6476E+00	0.4130E-05	0.1689E+01
IMF	0.02	0.38100E+01	82.5443	33.1366	1.5500	0.3448E+01	0.0000E+00	0.2772E+00	0.6987E+00	0.4510E-05	0.1822E+01
IMF	0.02	0.38200E+01	81.6059	32.7580	1.5500	0.3702E+01	0.0000E+00	0.2977E+00	0.7502E+00	0.4900E-05	0.1956E+01
IMF	0.02	0.38300E+01	80.6921	32.3893	1.5500	0.3957E+01	0.0000E+00	0.3182E+00	0.8021E+00	0.5301E-05	0.2091E+01
IMF	0.02	0.38400E+01	79.8017	32.0300	1.5500	0.4214E+01	0.0000E+00	0.3389E+00	0.8543E+00	0.5713E-05	0.2227E+01

Table 3, we calculate the stellar mass that corresponds to the stellar mean-lifetime  $\tau(m) = t$ . Interpolating in table 4 we obtain  $m_{\text{He}}$ , i.e. the mass of the star at  $X_{\text{H}}=0$ . We use this value of  $m_{\text{He}}$  to interpolate with the adequate value of mass in the explosive yields from WLW95/WLW93 and thus to calculate the stellar yields that correspond to this star. The yields are then multiplied by the number of stars given by  $\Phi(m)$  for the initial (zero age main sequence) mass of the star.

Because the production of elements given by WLW93 and

WLW95 is calculated only for stars with  $Z=0.02$  we have assumed that the relative yields for the other two abundances ( $Z=0.008$  and  $0.05$ ) of the high mass loss rate case are similar. Therefore we have calculated from the total ejected masses (the new elements and old ones) given by WLW93 and WLW95, the stellar yields, as new elements ejected by supernova as:

$$p_i = m_{\text{ej}} - (m_* - m_{\text{rem}}) * X_{i,0} \quad (3)$$



**Figure 9.** Evolution of the total abundances of the ejecta of a young stellar cluster with a Salpeter IMF due to stellar winds and supernova. Stellar wind contribution: Blue long dash lines. supernova contribution: Short dashed green lines. Total: Red solid line. The dotted grey line marks the solar abundance in each panel. The initial abundances are from top to bottom  $Z=0.05, 0.02, 0.008, 0.004, 0.0004, 0.0001$ . The elemental abundances are from left to right for He/H, C/H, N/H and O/H.

where  $X_{i,0}$  are the elemental abundances for each element  $i$  corresponding to  $Z=0.02$ , and  $m_{\text{rem}}$  is the mass of the remnant.

Then, we recalculated the ejected masses for each  $Z$  as:

$$mej_i = p_i + (m_* - m_{\text{rem}}) * X_{i,0} \quad (4)$$

for abundances  $Z=0.008$  and  $0.05$  using the same stellar yield  $p_i$  and substituting  $X_{i,0}$  with the corresponding values.

The instantaneous mass fraction for He, C, N and O for the supernova ejecta are presented in Fig. 7. Since the ejected mass has no H for supernovaIb/c, we show all abundances as total mass fraction, as before. The dotted line indicates the reference value for  $Z=0.02$ . Each color indicates a different metallicity with the same coding than in previous figures 3 and 4. For the three lowest  $Z$  only WW95 has been used, and so the evolution follows a continuous line. When  $Z \geq 0.008$  we see the change from the ejecta of supernovaIb (originally WR stars), following WLW93/WLW95 stellar yields, to the supernovaII from WW95 ejecta as a sharp vertical line. The first ones produce less He and N and more C and O than the second ones. This behavior is expected given that these stars ejected large quantities of He and N before to explode as supernova, during the stellar winds phase.

Table 5 gives the accumulated ejected masses by the supernovaIb/c and supernovaII explosions in each time step. For each IMF and metallicity given in columns 1 and 2 we show the time in column 3, the mass of the star which dies in this time in column 4, the mass of the He core in column 5, the remnant mass in column 6, the total ejected mass in column 7, and the ejected masses of H to O in columns 8 to 12.

The evolution of the accumulated or total abundances due to supernova ejections is illustrated in Fig. 8. A large increase in the O and C abundances is clearly seen at 4-6 Myr corresponding to the start of the supernova activity. After that there is a steady decrease reaching values around 2 times the initial values after almost 20 Myr. The He and N abundances, however, do not have an important contribution of supernovaIb and they maintain a constant high level after about 5 Myr due to the contribution of supernovaII with lower mass progenitors.

#### 4 THE TOTAL ABUNDANCES OF THE CLUSTER EJECTA

In this section we show the evolution of the stellar cluster abundances obtained by adding both contributions, winds and supernova explosions ejections.

In Fig. 9 we show the time evolution of the abundances. There we plot the contribution of winds by long dashed (blue) lines, the contribution coming from supernova with short-dashed (green) lines and the total abundances with solid (red) lines. For He both contributions are more or less similar at the end of 20 Myr when  $Z \geq 0.004$ , so the abundance is a factor of two if wind ejections are considered compared to the usual calculations performed with supernova productions only. For the two lowest metallicities the ejected masses are a factor 2 or 3 smaller.

We see that stellar winds produce high abundances of C and O only for  $Z \geq 0.004$ . The level of  $12+\log(\text{O}/\text{H})$  doesn't increase for  $Z \leq 0.004$ , while for higher  $Z$  it reaches almost two orders of magnitude larger. N, however, shows higher abundances than expected for all metallicities, even for the two lowest ones. Although these results are not unexpected, since they are due to the mass loss rate law that depends on  $Z$ , these abundances, not calculated

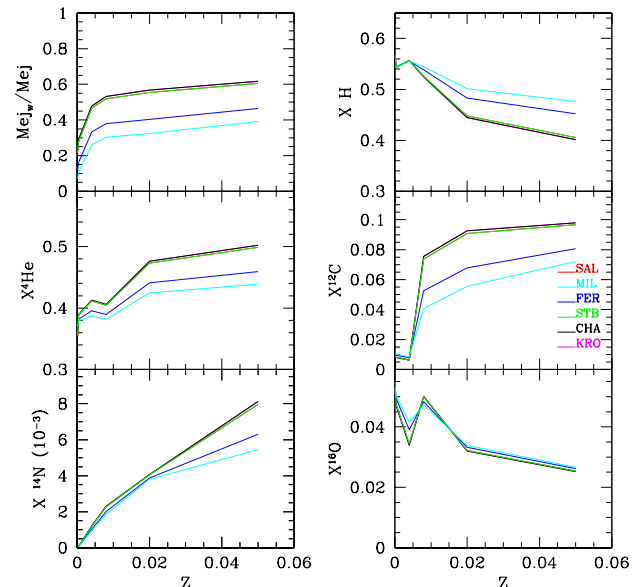


**Figure 10.** The dependence of the final ejected masses with the metallicity for different IMFs as labelled

before, may have important consequence over the interpretation of observations of HII regions.

When we analyze the same plots for supernovae, we see that now C and O show very high abundances, compared with the reference values, mainly for  $Z \leq 0.004$ , while He and N are roughly in the expected level for its metallicity. C and O are primary elements, produced directly from He created in the star. Therefore, their production is expected to be independent of the initial composition, whereas N is a secondary element produced in the CNO cycle at the expense of the initial C and O, so it is reasonable that it scales with the initial abundances.

A summary of these considerations is in Tables 6 and 7 where the accumulated masses ejected after 20 Myr by winds and by supernovae are given. In each one we give for each IMF and each metallicity the total mass ejected in  $M_{\odot}$  and then the contributions of each element, H, He, C, N and O proceeding from stellar winds and from supernovae, respectively.

For C the contribution of winds is essential, the supernovae contribution being a factor of 10 smaller except for the lowest metallicities ( $Z=0.0001, 0.0004$  and  $0.004$ ) for which the ejected masses are insignificant. Also for N only a small contribution is due to supernovae, at the end of the evolution, compared with the wind ejecta. For O the supernovae contribution is as important as the one from winds, particularly after 10 Myr of evolution. Therefore, the contributions of stellar winds to all abundances seems to be essential and must be taken into account in the evolution of stellar clusters and also in the galaxy evolution models in order to interpret adequately the data.

We show the final results for different IMFs in Fig. 10. There the fraction of mass ejected in the wind phase in panel a) and the final abundances in panels b) to d) are represented as a function of  $Z$  for the 6 IMFs of this work. Results for MIL and FER show the smallest abundances of He, C and N, and the highest H values. The other IMFs show results very similar, lower than MIL and FER in H, higher for the other elements. In any case differences among IMFs results are relatively small.

**Table 6.** Total masses ejected by stellar winds for a cluster at the end of the wind phase for all abundances and IMFs.

IMF	Z	mej ( $M_{\odot}$ )	H ( $M_{\odot}$ )	He ( $M_{\odot}$ )	C ( $M_{\odot}$ )	N ( $M_{\odot}$ )	O ( $M_{\odot}$ )
SAL	0.0001	12787	9363	3423	0	0	0
SAL	0.0004	18080	10881	7453	1	4	2
SAL	0.0040	41407	24726	18598	17	71	47
SAL	0.0080	52781	27930	22485	6933	160	2157
SAL	0.0200	62677	24161	34006	9683	269	1392
SAL	0.0500	70809	22410	40487	10853	759	1446
MIL	0.0001	2862	2106	753	0	0	0
MIL	0.0004	4362	2751	1646	0	1	1
MIL	0.0040	13721	8515	5656	7	21	18
MIL	0.0080	17733	10159	6807	1920	47	636
MIL	0.0200	21829	9598	10953	3253	85	461
MIL	0.0500	26913	9890	13988	4567	218	599
FER	0.0001	2190	1607	582	0	0	0
FER	0.0004	3200	1968	1268	0	1	0
FER	0.0040	8553	5211	3679	4	14	10
FER	0.0080	10966	6058	4422	1316	31	422
FER	0.0200	13278	5498	6918	2021	54	288
FER	0.0500	15719	5413	8538	2556	146	337
MAR	0.0001	32920	20437	7472	0	1	1
MAR	0.0004	46307	23750	16270	2	8	4
MAR	0.0040	98511	53958	40587	37	155	102
MAR	0.0080	128362	60948	49078	15132	349	4709
MAR	0.0200	151042	52724	74216	21128	587	3038
MAR	0.0500	169237	48903	88359	23681	1656	3156
CHA	0.0001	19514	14286	5227	0	1	1
CHA	0.0004	27528	16540	11381	1	5	3
CHA	0.0040	62281	37132	28066	25	107	70
CHA	0.0080	79380	41850	33976	10484	242	3254
CHA	0.0200	94122	36074	51222	14535	406	2093
CHA	0.0500	105977	33317	60835	16132	1148	2155
KRO	0.0001	18392	13464	4926	0	0	1
KRO	0.0004	25946	15589	10727	1	5	3
KRO	0.0040	58700	34998	26452	24	101	66
KRO	0.0080	74816	39444	32023	9881	228	3067
KRO	0.0200	88711	34000	48277	13699	383	1973
KRO	0.0500	99885	31402	57338	15205	1082	2031
STB	0.0001	25645	18777	6865	0	1	1
STB	0.0004	36260	21821	14947	1	7	4
STB	0.0040	83041	49587	37297	34	142	94
STB	0.0080	105851	56013	45094	13903	321	4326
STB	0.0200	125698	48455	68198	19418	540	2792
STB	0.0500	142007	44943	81196	21766	1521	2900

## 5 CONCLUSIONS

We have computed the evolution of the total mass ejected and the elemental abundances of He, C, N and O for young stellar clusters of  $10^6 M_{\odot}$  for 6 IMFs and for 6 different initial metallicities.

Both stellar wind and supernova contribution to the ejecta are included in the computations. The supernova contribution include the classical gravitational collapse from Woosley & Weaver (1995) for low mass progenitors plus the yields calculated by Woosley et al (1993) and Woosley, Langer & Weaver (1995) for stars more massive than  $30 M_{\odot}$  and with  $Z \geq 0.008$  that reach the supernova stage after completely losing their H envelope.

The abundances of the ejecta obtained by adding both contributions show important differences in comparison with the standard method which uses only supernovae yields without taking into account the stellar wind yields and/or the difference in the supernovae

**Table 7.** Total masses ejected by supernova for a cluster at the end of the supernova phase for each computed metallicity.

IMF	Z	Mej ( $M_{\odot}$ )	H ( $M_{\odot}$ )	He ( $M_{\odot}$ )	C ( $M_{\odot}$ )	N ( $M_{\odot}$ )	O ( $M_{\odot}$ )
SAL	0.0001	46230	24090	17510	521	2	3089
SAL	0.0004	46520	24230	17670	529	2	3058
SAL	0.0040	47510	24800	17980	549	35	3018
SAL	0.0080	49020	25610	18690	563	72	2934
SAL	0.0200	50460	26510	19530	581	189	2246
SAL	0.0500	46240	25050	17870	468	173	1522
MIL	0.0001	36540	19470	13850	410	1	2093
MIL	0.0004	36860	19650	13990	416	1	2076
MIL	0.0040	38750	20630	14650	443	29	2164
MIL	0.0080	40880	21760	15570	463	62	2138
MIL	0.0200	45560	24180	17660	492	171	1821
MIL	0.0500	41880	22880	16200	390	157	1236
FER	0.0001	16310	8635	6179	183	1	978
FER	0.0004	16440	8706	6238	186	1	969
FER	0.0040	17150	9078	6484	196	13	994
FER	0.0080	17990	9531	6855	205	27	977
FER	0.0200	19690	10420	7626	216	74	808
FER	0.0500	18080	9860	6991	172	68	548
MAR	0.0001	100900	52600	38240	1138	4	6752
MAR	0.0004	101600	52900	38590	1156	4	6687
MAR	0.0040	103700	54120	39270	1198	77	6596
MAR	0.0080	107000	55890	40800	1230	158	6410
MAR	0.0200	110100	57830	42610	1269	412	4903
MAR	0.0500	100900	54660	38990	1022	377	3323
CHA	0.0001	66310	34510	25120	748	3	4476
CHA	0.0004	66720	34700	25340	759	3	4430
CHA	0.0040	68000	35440	25750	786	51	4357
CHA	0.0080	70060	36550	26710	806	103	4231
CHA	0.0200	71700	37640	27750	830	269	3215
CHA	0.0500	65690	35570	25380	670	246	2179
KRO	0.0001	62490	32520	23670	705	2	4218
KRO	0.0004	62890	32700	23880	716	3	4176
KRO	0.0040	64090	33400	24270	741	48	4107
KRO	0.0080	66040	34450	25180	760	97	3988
KRO	0.0200	67580	35470	26150	782	253	3031
KRO	0.0500	61920	33520	23920	631	232	2054
STB	0.0001	92710	48320	35120	1046	4	6195
STB	0.0004	93300	48600	35430	1061	4	6133
STB	0.0040	95280	49730	36070	1100	71	6052
STB	0.0080	98310	51360	37480	1130	145	5883
STB	0.0200	101200	53160	39170	1165	379	4504
STB	0.0500	92740	50240	35840	939	347	3053

yields resulting from the huge mass loss affecting the pre-supernova evolution.

In particular:

- The composition of the ejected matter is determined mostly by supernova at low metallicities and by stellar winds at around Solar metallicities.
- The total mass ejected by stellar winds ranges from about 1% of the initial cluster mass for the lowest metallicity model to about 6% for the  $\sim$  Solar abundance ones of the total mass of the cluster for a Salpeter IMF.
- The total mass ejected by supernova is  $\sim$ 5% of the total mass of the cluster for all initial metallicities.
- At high metallicities the proportion of the mass ejected by the winds phase is around 40-60% of the total ejecta.
- There is a large increase in the abundance of He, C, O and N after 2.5 Myr with O and C abundances being the most extreme.

The O abundance jumps almost two orders of magnitude between 2.5 and 4 Myr in our lowest metallicity model and about 3 times for the solar abundance model. Between 2 and 3 Myr, the C abundance increases between 10 and 30 times its initial value depending on the initial abundance.

- He and N show more moderate jumps than C and O in their abundance between 2.5 and 4 Myr. He abundance increases almost 3 times for the solar value models and about 2 times for  $Z = 0.0004$ . On the other hand N shows jumps of about 5 times for all abundances. For cluster ages  $t < 10$  Myr, He and N enrichment is mainly due to the stellar winds.

These huge variations in the abundances of the ejecta of a stellar cluster can have a profound effect in the hydrodynamical evolution of the ISM. The high metallicity of the young cluster ejecta will lead to extremely short cooling times with important consequences for the subsequent feedback.

On the other hand, one should keep in mind the main shortcomings and uncertainties of our models:

Because present stellar evolutionary models with mass loss do not include the supernova phase and supernova models do not cover a range in initial abundances, our adopted values for the supernova yields of the most massive stars are only approximate.

Binary evolution is not considered. It is known that in young massive clusters perhaps all massive stars are in binary or multiple systems, but it is not clear how the presence of a companion would affect the properties of wind of a massive star.

The effect of stellar rotation is not included in the stellar evolution models we have used. Again, as in the case of binaries, is not clear at this stage how rotation would affect the wind of a massive star.

In spite of these warnings, our models should be useful for the interpretation of the evolution of the ISM in star forming galaxies. The resulting tables are available in electronic format.

## 6 ACKNOWLEDGMENTS

This work has been partially supported by DGICYT grant AYA2010-21887-C04-02. Also, by the Comunidad de Madrid under grant CAM S2009/ESP-1496 (AstroMadrid) and by the Spanish MICINN under the Consolider-Ingenio 2010 Program grant CSD2006-00070: First Science with the GTC<sup>3</sup>. RT is grateful to the Mexican Research Council (CONACYT) for supporting this research under grants CB-2006-49847, CB-2007-01-84746 and CB-2008-103365-F. We would like to thank Elena Terlevich and the referee Rafael Hirschi for for many suggestions that greatly improved this paper. Dedicated to the memory of M.F.B.

## REFERENCES

Asplund M., Grevesse N., Sauval A. J., Scott P., 2009, *ARA&A*, 47, 481  
 Bressan A., Fagotto F., Bertelli G., Chiosi C. 1993, *A&AS*, 100, 647  
 Cerviño, M., & Luridiana, V. 2006, *A&A*, 451, 475  
 Cerviño, M., & Luridiana, V. 2004, *A&A*, 413, 145  
 Chabrier G., 2003, *ApJ*, 586, L133  
 Chieffi A., Limongi M., 2004, *ApJ*, 608, 405

Dray L. M., Tout C. A., 2003, *MNRAS*, 341, 299  
 Dray L. M., Tout C. A., Karakas A. I., Lattanzio J. C., 2003, *MNRAS*, 338, 973  
 Fagotto F., Bressan A., Bertelli G., & Chiosi C. 1994a, *A&AS*, 105, 29  
 Fagotto F., Bressan A., Bertelli G., Chiosi C., 1994b, *A&AS*, 104, 365  
 Ferrini F., Penco U., Palla F., 1990, *A&A*, 231, 391  
 Fröhlich C., et al., 2006, *ApJ*, 637, 415  
 Heger A., & Woosley S. E., 2010, *ApJ*, 724, 341  
 Hirschi R., Meynet G., Maeder A., 2005, *NuPhA*, 758, 234  
 Hirschi R., 2007, *A&A*, 461, 571  
 Kobayashi C., Umeda H., Nomoto K., Tominaga N., Ohkubo T., 2006, *ApJ*, 653, 1145  
 Kobulnicky H. A., Skillman E. D., Roy J.-R., Walsh J. R., Rosa M. R., 1997, *ApJ*, 477, 679  
 Kobulnicky, H. A., & Skillman, E. D. 1998, *ApJ*, 497, 601  
 Kroupa P., 2001, *MNRAS*, 322, 231  
 Leitherer C., et al., 1999, *ApJS*, 123, 3  
 Limongi M., Chieffi A., 2003, *ApJ*, 592, 404  
 López-Sánchez, Á. R., & Esteban, C. 2010, *A&A*, 517, A85  
 Maeder A., 1992, *A&A*, 264, 105  
 Meynet G., Maeder A., 2002, *A&A*, 390, 561  
 Miller G. E., Scalo J. M., 1979, *ApJS*, 41, 513  
 Portinari L., Chiosi C., Bressan A., 1998, *A&A*, 334, 505  
 Raymond, J. C., Cox, D. P., & Smith, B. W. 1976, *ApJ*, 204, 290  
 Rauscher T., Heger A., Hoffman R. D., Woosley S. E., 2002, *ApJ*, 576, 323  
 Salpeter, E.E., 1955 *ApJ*, 121, 161  
 Silich, S. A., Tenorio-Tagle, G., Terlevich, R., Terlevich, E., & Netzer, H. 2001, *MNRAS*, 324, 191  
 Tenorio-Tagle, G. 1996, *AJ*, 111, 1641  
 Umeda H., Nomoto K., 2002, *ApJ*, 565, 385  
 van Zee, L., & Haynes, M. P. 2006, *ApJ*, 636, 214  
 Woosley, S. E., Langer, N., & Weaver, T. A. 1993, *ApJ*, 411, 823  
 Woosley, S. E., Langer, N., & Weaver, T. A. 1995, *ApJ*, 448, 315  
 Woosley, S. E. & Weaver, T. A. 1995, *ApJS*, 101, 181

<sup>3</sup> <http://www.iac.es/consolider-ingenio-gtc>